INTERNATIONAL JOURNAL FOR NUMERICAL METHODS IN ENGINEERING
Int. J. Numer. Meth. Engng 2010; **84**:27–46
Published online 29 March 2010 in Wiley Online Library (wileyonlinelibrary.com). DOI: 10.1002/nme.2881

Localized electrical current propagation in anisotropically perturbed atmospheres

T. I. Zohdi*, †

Department of Mechanical Engineering, 6195 Etcheverry Hall, University of California, Berkeley, CA 94720-1740, U.S.A.

SUMMARY

The trajectory of free atmospheric electrical currents, such as lightning and sparks, is strongly influenced by microscale events that occur at the current front. In particular, highly conductive pathways can occur at the free surface front due to *dielectric breakdown*. The specific directions of the local pathways are minutely perturbed, due to the gaseous, disordered, nature of the media at the small scale. This results in highly conductive, anisotropically perturbed, continuum-level properties at the electrical current front. In this work, a model is developed to investigate the role of the resulting anisotropically perturbed conductivity at the propagation front on the overall trajectory of free atmospheric electrical currents. The approach is to relate the electrical current velocity to the local anisotropic conductivity at the propagation front and the surrounding electric field. The conductive anisotropy is decomposed into an isotropic 'base state' and an anisotropic perturbation. The current trajectory is shown to be governed by a set of non-linear differential equations, for which a numerical solution scheme is developed. The difference between paths taken through anisotropically perturbed and isotropic media is analytically bounded and quantified numerically as a function of the magnitude of the anisotropic perturbation. The analysis and numerical experiments indicate that, in a statistical sense, the difference in the paths taken in anisotropically perturbed and isotropic media depends quasilinearly on the perturbation magnitude.

Received 18 August 2009; Revised 31 January 2010; Accepted 1 February 2010

KEY WORDS: electrical current; perturbed trajectory; atmosphere

1. INTRODUCTION

The trajectory of a free electrical discharge in a gaseous atmosphere, referred here as a 'jet', is strongly influenced by the local conditions at the current front. Examples include lightning and sparks (Figure 1). To a large extent, the jet trajectory propagation is influenced by inhomogeneities in the local microscopic properties at the electrical free surface front 'tip' (Figure 2). Continuum properties at the electrical front tip, such as the conductivity, are determined by what is sometimes termed as *dielectric breakdown*, whereby, for sufficiently strong electrical fields, an initially poor

*Correspondence to: T. I. Zohdi, Department of Mechanical Engineering, 6195 Etcheverry Hall, University of California, Berkeley, CA 94720-1740, U.S.A.
†E-mail: zohdi@me.berkeley.edu

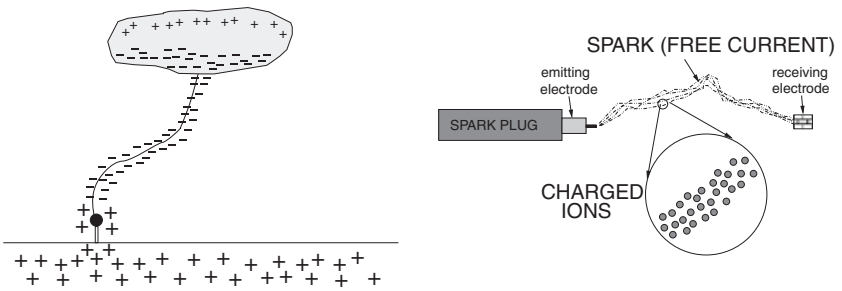

Figure 1. Examples of free electrical currents. Left: a lightning strike. Right: a spark comprising of a charged ion jet.

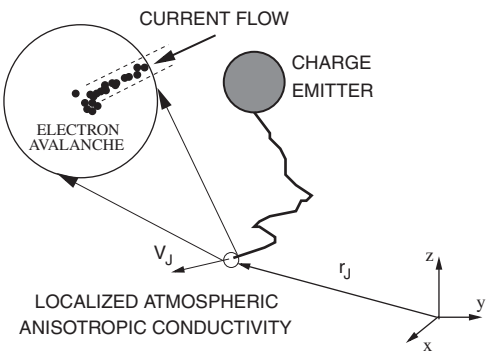

Figure 2. The current flow at the electrical front 'tip'.

conductor can become an extremely good conductor. The process occurs when an applied field is strong enough to accelerate free electrons that are present in a gas so that they attain energies sufficiently large enough to dislodge other electrons in initially neutral molecules. The result is a collection of positively charged ions and free electrons. The dislodged electrons then repeat the procedure in a chain-like reaction manner leading to an *electron avalanche*, which results in highly conductive, anisotropic, properties at the electrical front tip. The investigation of dielectric breakdown has a long history dating back to at least to Townsend (1914) [1]. A detailed discussion of the phenomenon can be found in Inan and Inan [2]. Since the local microstructure at the electric field front tip is inhomogeneous (essentially it is a random medium), the (homogenized) continuum scale properties, such as the conductivity, can be highly directionally dependent and, thus, anisotropic on the continuum scale.[‡]

Clearly, these effects can influence a free current's trajectory, which is the primary theme of this paper. There are a number of applications in both the natural sciences and industry where the characterization of the path of localized electrical currents ('filaments') in gases is of interest. Two important applications are (1) lightning and (2) spark propagation (ignition systems) in internal combustion engines, which are now briefly discussed.

[‡]Measurements of local variations in atmospheric conductivity can be found in, for example, Bering *et al.* [3], Holzworth *et al.* [4], Pinto *et al.* [5], Hu *et al.* [6].

DOI: 10.1002/nme

1.1. Relevance to natural phenomena: lightning

Generally speaking, lightning is an atmospheric discharge of electricity that is associated with thunderstorms. It is commonly thought that the formation of ice inside a cloud is critical for the initiation of lightning, since this can cause a separation of positive and negative charges within the cloud, leading to a significant potential difference between the earth (or objects on its surface) and the lower section of a cloud. If conditions are appropriate, an electrical discharge will occur. One hypothesis is based on electrostatic induction, where it is asserted that charge separation occurs, requiring strong updrafts which carry water droplets upward and supercooling them to between -10 and -20°C. These droplets collide with ice crystals to form a soft ice–water mixture called graupel. The collisions result in a slightly positive charge being transferred to ice crystals, and a slightly negative charge to the graupel. Updrafts drive the less heavy ice crystals upwards, causing the cloud top to accumulate positive charge. Gravity causes the heavier negatively charged graupel to fall toward the middle and lower portions of the cloud, building up a negative charge. Charge separation and accumulation continue until the electrical potential becomes sufficient to initiate a lightning discharge, which occurs when the distribution of positive and negative charges forms a sufficiently strong electric field. Another hypothesis is based on a polarization mechanism that occurs in two stages, namely, (1) falling droplets of ice and rain become electrically polarized as they fall through the Earth's natural electric field and (2) colliding ice particles become charged by electrostatic induction. Atmospheric conditions such as humidity and pressure can effect this process. Furthermore, it has also been proposed that solar induced activity such as gamma ray bursts (leading to ionization of air molecules), the solar wind, charged plasma bulidup etc, can influence lightning behavior.[§] Clearly, there is not one root cause for lightning initiation. Detailed discussions on the various origins of favorable conditions for lightning can be found in Rakov and Uman [7], Demirkol *et al.* [8], Uman [9], Fishman *et al.* [10], Inan *et al.* [11] and Inan and Inan [2]. *In this paper, we remove ourselves from the discussion of the origin of the charge build up and discharge, and focus our attention on the mathematical description of the current trajectory.* Specifically, this work attempts to connect the degree of local atmospheric anisotropy to the trajectory of a jet. However, before proceeding with the analysis, we discuss another important application, namely ignition in combustion processes.

1.2. Relevance to industry: internal combustion systems

Many modern devices, such as ignition systems in internal combustion engines, owe a significant amount of their success to the control of localized electrical sparks ('jets'). Specifically, the development of ignition systems for ultra lean fuels, such as ethanol, is an area of high interest for spark (localized electrical jet) control. Generally, because of the advancements in sensor and control systems in harsh environments (see Azevedo *et al.* [12] and Schwartz [13]), the real time adjustment of *in situ* ignition systems is becoming viable, and is an area of active research. In particular, spark manipulation and control via electromagnetic (microwave) techniques is now possible. Such approaches are important for developing hybrid systems involving compression ignition direct injection (CIDI) and homogeneous charge compression ignition (HCCI) engine platforms, in order to improve the performance of a broad class of engines. Such systems can lead

[§] Volcanic eruptions producing dust and other natural events involving atmospheric electrical activity, such as intense forest fires, can enhance the possibility of lightning strikes.

DOI: 10.1002/nme

to improved efficiency by igniting ultra lean fuels at low temperatures where standard compression engines are limited and misfiring occurs. In particular, it has recently been proposed that shortly after a spark (charged plasma) is discharged into the combustion chamber, a microwave is released to disperse the spark throughout the combustion chamber. Because of the dispersion of the spark throughout the combustion chamber, the ignition system relies far less on the propagation of the flame to ignite the fuel and, hence, far leaner fuels may be employed without misfire occurring. Until recently, the detailed control of sparks has been unreachable. However, as mentioned earlier, within the last decade microtechnology, in particular microelectronic sensors, has made it possible for engineers to control combustion events via the propagation of sparks and flame fronts. This is a huge field, and we list a cross-section of that research for the interested reader: Ikeda *et al.* [14], Kaneko *et al.* [15], Liepold *et al.* [16], Phelps [17], Aleiferis *et al.* [18], Johansson [19], Kogoma [20], Phuoc [21], Morsy *et al.* [22], Morsy *et al.* [23] Ma *et al.* [24], Ma *et al.* [25], Mohamed *et al.* [26], Weinberg and Wilson [27], Dale *et al.* [28], Ronney [29], Beduneau [30], Chen and Lewis [31], Phuoc [32], Kim *et al.* [33], Ombrello and Ju [34], Mintoussov *et al.* [35], Korolev and Matveev [36], Kim, *et al.* [33], Esakov, *et al.* [37], Linkenheil *et al.* [38], Linkenheil *et al.* [39], Ikeda, *et al*. [40], Kawahara *et al.* [41], Mehresh *et al.* [42], Bogin *et al.* [43], and Prager *et al.* [44]. A further understanding of what influences the propagation of localized electrical jets in fuel–air mixtures, and general gases, is critical for the improvement of combustion processes.

2. LOCALIZED CURRENT MOVEMENT

By definition, electric current is the rate of transport of electric charge past a specified point or surface. The current density is denoted $\boldsymbol{J}$.[¶] When in a medium, collisions slow down the charge carrying particles (such as ions). On average, the random velocity components, due to random collisions, cancel one another out and we are left with a drift velocity, which is proportional to the electric field. For an ensemble of charged particles, one can write[‖]

$$\boldsymbol{J} = \sum_{i=1}^{\text{particles}} q_i \mathscr{V}_i \stackrel{\text{def}}{=} \mathscr{P}\boldsymbol{V} \stackrel{\text{def}}{=} \boldsymbol{\sigma}\cdot\boldsymbol{E}, \tag{1}$$

where q_i is the charge of particle i, $\mathscr{V}_i$ is the velocity of particle i, $\boldsymbol{V}$ is an average (group) drift velocity, $\mathscr{P}$ is the overall charge of the stream of charge carriers and $\boldsymbol{\sigma}$ is the conductivity tensor. Let us consider the decomposition

$$\boldsymbol{E} = \underbrace{\boldsymbol{E}_{\text{J}}}_{\text{jet}} + \underbrace{\boldsymbol{E}_{\text{E}}}_{\text{external}}, \tag{2}$$

where $\boldsymbol{E}_{\text{J}}$ is the intrinsic electrical field associated with the jet (due to its charged particles) and $\boldsymbol{E}_{\text{E}}$ is the electrical field associated with external sources, which will be discussed in more detail

[¶] The total (normal flux) current is $I = \int_A \boldsymbol{J}\cdot\boldsymbol{n}\,\mathrm{d}A$.

[‖] The expected velocity range of the charged particles is sufficiently small (relative to the speed of light), therefore self-induced magnetic fields will be considered negligible. External magnetic fields are also neglected.

DOI: 10.1002/nme

later in the paper. The velocity vector of the jet of charged particles dictates the electric field of the jet

$$\boldsymbol{E}_{\mathrm{J}} = E_o \frac{\boldsymbol{V}_{\mathrm{J}}}{\|\boldsymbol{V}_{\mathrm{J}}\|} = E_o \boldsymbol{s}_{\mathrm{J}}, \tag{3}$$

where $E_o = \|\boldsymbol{E}_{\mathrm{J}}\|$ is assumed to be of constant (magnitude), $\boldsymbol{V}_{\mathrm{J}}$ is the velocity of the electrical jet and $\boldsymbol{s}_{\mathrm{J}}$ is the jet trajectory (tangent to path) vector. Therefore, we have

$$\boldsymbol{V}_{\mathrm{J}} = \frac{1}{\mathscr{P}} \boldsymbol{\sigma} \cdot (\boldsymbol{E}_{\mathrm{J}} + \boldsymbol{E}_{\mathrm{E}}). \tag{4}$$

The position vector of the jet is related to the velocity via $\dot{\boldsymbol{r}}_{\mathrm{J}} = \boldsymbol{V}_{\mathrm{J}}$, which can be numerically solved simultaneously with the other system equations. This is discussed later in the presentation.

3. CONDUCTIVE ANISOTROPY

On the continuum level, it is standard to assume that a conductive energy function per unit volume exists, a non-negative function denoted W. A linear constitutive relation for the current can be derived by differentiating an energy function with respect to the electric field, $\boldsymbol{J} = \partial W / \partial \boldsymbol{E}$, where $W \approx c_0 + \mathbf{c}_1 \cdot \boldsymbol{E} + \frac{1}{2} \boldsymbol{E} \cdot \boldsymbol{\sigma} \cdot \boldsymbol{E} + \mathscr{O}(\|\boldsymbol{E}\|^3)$, which implies that $\boldsymbol{J} \approx \mathbf{c}_1 + \boldsymbol{\sigma} \cdot \boldsymbol{E} + \mathscr{O}(\|\boldsymbol{E}\|^2)$. We are free to set $c_0 = 0$ (it is arbitrary) to have zero energy at zero $\boldsymbol{E}$, and furthermore, we assume that no electrical current exists in the reference state ($\mathbf{c}_1 = \mathbf{0}$); we obtain a general linear anisotropic relation between the electrical current and the electric field, $\boldsymbol{J} = \boldsymbol{\sigma} \cdot \boldsymbol{E}$. In general, $\boldsymbol{\sigma}$ has nine independent constants, since it is a second order tensor relating three components of electric flux to electric field

$$\underbrace{\begin{Bmatrix} J_1 \\ J_2 \\ J_3 \end{Bmatrix}}_{\stackrel{\text{def}}{=} \boldsymbol{J}} = \underbrace{\begin{bmatrix} \sigma_{11} & \sigma_{12} & \sigma_{13} \\ \sigma_{21} & \sigma_{22} & \sigma_{23} \\ \sigma_{31} & \sigma_{32} & \sigma_{33} \end{bmatrix}}_{\stackrel{\text{def}}{=} \boldsymbol{\sigma}} \underbrace{\begin{Bmatrix} E_1 \\ E_2 \\ E_3 \end{Bmatrix}}_{\stackrel{\text{def}}{=} \boldsymbol{E}}. \tag{5}$$

Typically, different media are classified according to the number of independent constants in $\boldsymbol{\sigma}$. Depending on the medium's microstructure, it can be shown that the components of $\boldsymbol{\sigma}$ may be written in terms of anywhere between nine and one independent parameters. The existence of a strictly positive energy function implies that $\boldsymbol{\sigma}$ must have positive eigenvalues at every point in the domain (system atmosphere). The existence of a scalar energy function forces $\boldsymbol{\sigma}$ to be symmetric, in other words, $W = \frac{1}{2} \boldsymbol{E} \cdot \boldsymbol{\sigma} \cdot \boldsymbol{E} = \frac{1}{2} (\boldsymbol{E} \cdot \boldsymbol{\sigma} \cdot \boldsymbol{E})^{\mathrm{T}} = \frac{1}{2} \boldsymbol{E} \cdot \boldsymbol{\sigma}^{\mathrm{T}} \cdot \boldsymbol{E}$, which implies $\boldsymbol{\sigma}^{\mathrm{T}} = \boldsymbol{\sigma}$. Consequently, $\boldsymbol{\sigma}$ has only six free constants. The non-negativity of W imposes the restriction that $\boldsymbol{\sigma}$ remains positive definite. At this point, based on many factors that depend on the local fine scale features of the atmosphere, the conductivity will have various directional 'biases'. For example, consider a fixed Cartesian triad ($x_1 - x_2 - x_3$), with an $x_2 - x_3$ plane of symmetry. A plane of symmetry implies that the medium has the same properties with respect to that plane. Therefore, we should be able to exchange ('flip') the axes with respect to that plane, and have no change in the constitutive law. By definition, a plane of symmetry exists at a point where the material constants have the same value for a pair of coordinate systems. An axis of symmetry of order K exists at a point when there are sets of equivalent conductive directions which can be superposed by a rotation through an angle $2\pi/K$ about an axis. In order to determine conductive symmetry first, we rotate the current

DOI: 10.1002/nme

($\boldsymbol{J}$) and electric field ($\boldsymbol{E}$) vectors $\hat{\boldsymbol{J}}=\boldsymbol{Q}\cdot\boldsymbol{J}$ and $\hat{\boldsymbol{E}}=\boldsymbol{Q}\cdot\boldsymbol{E}$, yielding the transformed system $\hat{\boldsymbol{J}}=\hat{\boldsymbol{\sigma}}\cdot\hat{\boldsymbol{E}}$, which implies the following relationship $\boldsymbol{J}=(\boldsymbol{Q}^{-1}\cdot\hat{\boldsymbol{\sigma}}\cdot\boldsymbol{Q})\cdot\boldsymbol{E}$, where $\boldsymbol{Q}$ is a rotational transformation matrix. Imposing electrical symmetry dictates that the components of $\boldsymbol{\sigma}$ are invariant with respect to the transformation, hence, $\boldsymbol{\sigma}=\hat{\boldsymbol{\sigma}}$ and also $\boldsymbol{\sigma}=\boldsymbol{Q}^{-1}\cdot\hat{\boldsymbol{\sigma}}\cdot\boldsymbol{Q}=\boldsymbol{Q}^{-1}\cdot\boldsymbol{\sigma}\cdot\boldsymbol{Q}$. Therefore, all components that are not identical (after the transformation) must be zero if the medium has the assumed electrical symmetry. In this manner, one can eliminate components from a general anisotropic conductivity tensor. The central point of such symmetries is that in a new transformed state, $\boldsymbol{\sigma}$ should not change. If we consider a Cartesian $(x_1-x_2-x_3)$ coordinate system, by performing a series of rotational transformations about the axes, and enforcing material invariance yields an isotropic medium that can be written in the form $\boldsymbol{\sigma}=\sigma\mathbf{1}$, for the case where there exist an infinite number of planes, the material properties are equal in all directions (symmetry of order $K=\infty$). Therefore, representation by a single-material constant (σ) is possible. In this case we have

$$\boldsymbol{J}=\boldsymbol{\sigma}\cdot\boldsymbol{E}=\sigma\mathbf{1}\cdot\boldsymbol{E}=\sigma\boldsymbol{E} \tag{6}$$

where, under the assumption of a positive energy, we must have $\sigma>0$ to retain positive definiteness of $\boldsymbol{\sigma}$. See the Appendix for more details.

4. ELECTRICAL CURRENT PROPAGATION TRAJECTORY

Consider

$$\boldsymbol{V}_{\mathrm{J}}=\frac{1}{\mathscr{P}}\boldsymbol{\sigma}\cdot(\boldsymbol{E}_{\mathrm{J}}+\boldsymbol{E}_{\mathrm{E}})=\frac{1}{\mathscr{P}}\boldsymbol{\sigma}\cdot\left(E_o\frac{\boldsymbol{V}_{\mathrm{J}}}{\|\boldsymbol{V}_{\mathrm{J}}\|}+\boldsymbol{E}_{\mathrm{E}}\right). \tag{7}$$

Simple algebraic manipulations lead to

$$\underbrace{\left(\boldsymbol{\sigma}\frac{E_o}{\|\boldsymbol{V}_{\mathrm{J}}\|}-\mathscr{P}\mathbf{1}\right)}_{\stackrel{\mathrm{def}}{=}\boldsymbol{A}}\cdot\boldsymbol{V}_{\mathrm{J}}=-\boldsymbol{\sigma}\cdot\boldsymbol{E}_{\mathrm{E}}. \tag{8}$$

If $\boldsymbol{A}$ is invertible

$$\boldsymbol{V}_{\mathrm{J}}=-\boldsymbol{A}^{-1}\cdot(\boldsymbol{\sigma}\cdot\boldsymbol{E}_{\mathrm{E}}). \tag{9}$$

The above represents a set of non-linear implicit equations, which will be treated numerically shortly.

4.1. Special case: isotropic with no external source

In the special case when $\boldsymbol{\sigma}=\sigma_o\mathbf{1}$ and $\boldsymbol{E}_{\mathrm{E}}=\mathbf{0}$ (isotropic and no external fields), we obtain

$$\left(\frac{\sigma_o E_o}{\|\boldsymbol{V}_{\mathrm{J}}\|}-\mathscr{P}\right)\boldsymbol{V}_{\mathrm{J}}=\mathbf{0}. \tag{10}$$

Thus, for a non-trivial solution, we must have a constant velocity magnitude

$$\|\boldsymbol{V}_{\mathrm{J}}\|=\frac{\sigma_o E_o}{\mathscr{P}}. \tag{11}$$

Since the general (numerical) solution scheme will be cast in the form of $\boldsymbol{V}_{\mathrm{J}}^{i+1}=\mathscr{G}(\boldsymbol{V}_{\mathrm{J}}^{i})$, where $i=0,1,2,\ldots N$ are successive iterations and $\boldsymbol{V}_{\mathrm{J}}^{i=0}=\boldsymbol{V}_{\mathrm{J}}(t=0)$, the velocity trajectory will also

DOI: 10.1002/nme

remain unchanged and is

$$\boldsymbol{V}_{\mathrm{J}} = \frac{\sigma_o E_o}{\mathscr{P}} \boldsymbol{s}_{Jo}, \tag{12}$$

where $\boldsymbol{s}_{Jo} = \boldsymbol{V}_{\mathrm{J}}(t=0)/\|\boldsymbol{V}_{\mathrm{J}}(t=0)\|$ is the initial trajectory of the jet.

4.2. Special case: isotropic with an external source

In the special case when $\boldsymbol{\sigma} = \sigma_o \mathbf{1}$ (isotropic), we obtain

$$\boldsymbol{V}_{\mathrm{J}} = -\left(\frac{\sigma_o}{\dfrac{\sigma_o E_o}{\|\boldsymbol{V}_{\mathrm{J}}\|} - \mathscr{P}} \right) \boldsymbol{E}_{\mathrm{E}}. \tag{13}$$

Therefore, in the case of pure isotropy, the velocity will be aligned with the external electric field.

4.3. General case: perturbations from isotropy

Consider now deviations from anisotropy of the form ($\delta\boldsymbol{\sigma} = (\delta\boldsymbol{\sigma})^{\mathrm{T}}$)

$$\boldsymbol{\sigma} = \sigma_o \mathbf{1} + \delta\boldsymbol{\sigma}, \tag{14}$$

where

$$\boldsymbol{\sigma} \stackrel{\text{def}}{=} \begin{bmatrix} \sigma_o \pm \delta\sigma_{11} & \pm\delta\sigma_{12} & \pm\delta\sigma_{13} \\ \pm\delta\sigma_{21} & \sigma_o \pm \delta\sigma_{22} & \pm\delta\sigma_{23} \\ \pm\delta\sigma_{31} & \pm\delta\sigma_{32} & \sigma_o \pm \delta\sigma_{33} \end{bmatrix}, \tag{15}$$

and

$$\delta\boldsymbol{\sigma} \stackrel{\text{def}}{=} \begin{bmatrix} \delta\sigma_{11} & \delta\sigma_{12} & \delta\sigma_{13} \\ \delta\sigma_{21} & \delta\sigma_{22} & \delta\sigma_{23} \\ \delta\sigma_{31} & \delta\sigma_{32} & \delta\sigma_{33} \end{bmatrix}, \tag{16}$$

where $\delta\sigma_{ij}^{-} \leqslant \delta\sigma_{ij} \leqslant \delta\sigma_{ij}^{+}$ are random perturbations that reflect the local changes in the atmospheric conductivity. We remark that the 'perturbed' conductivity must always satisfy a positive definiteness requirement

$$\det(\boldsymbol{\sigma}) = \det(\sigma_o \mathbf{1} + \delta\boldsymbol{\sigma}) > 0. \tag{17}$$

4.4. Bounds/estimates on the trajectory deviation

At a given moment in time, let us consider the difference in the trajectories of a jet ($\boldsymbol{V}_{\mathrm{J}}$) encountering an anisotropic medium ($\boldsymbol{\sigma} = \boldsymbol{\sigma}_o + \delta\boldsymbol{\sigma}$, where $\boldsymbol{\sigma}_o = \sigma_o \mathbf{1}$), governed by

$$\boldsymbol{V}_{\mathrm{J}} = \frac{1}{\mathscr{P}} \boldsymbol{\sigma} \cdot \left(E_o \underbrace{\frac{\boldsymbol{V}_{\mathrm{J}}}{\|\boldsymbol{V}_{\mathrm{J}}\|}}_{\boldsymbol{s}_{\mathrm{J}}} + \boldsymbol{E}_{\mathrm{E}} \right) = \frac{1}{\mathscr{P}} \boldsymbol{\sigma} \cdot (E_o \boldsymbol{s}_{\mathrm{J}} + \boldsymbol{E}_{\mathrm{E}}) \Rightarrow \boldsymbol{s}_{\mathrm{J}} = \frac{1}{E_o} (\boldsymbol{\sigma}^{-1} \cdot \mathscr{P} \boldsymbol{V}_{\mathrm{J}} - \boldsymbol{E}_{\mathrm{E}}), \tag{18}$$

DOI: 10.1002/nme

and a jet ($\boldsymbol{V}_{\mathrm{J}}$) encountering an isotropic medium ($\boldsymbol{\sigma}_o = \sigma_o \mathbf{1}$), governed by

$$\boldsymbol{V}_{Jo} = \frac{1}{\mathscr{P}} \boldsymbol{\sigma}_o \cdot \left(E_o \underbrace{\frac{\boldsymbol{V}_{Jo}}{\|\boldsymbol{V}_{Jo}\|}}_{\boldsymbol{s}_{Jo}} + \boldsymbol{E}_{\mathrm{E}} \right) = \frac{1}{\mathscr{P}} \boldsymbol{\sigma}_o \cdot (E_o \boldsymbol{s}_{Jo} + \boldsymbol{E}_{\mathrm{E}}) \Rightarrow \boldsymbol{s}_{Jo} = \frac{1}{E_o} (\boldsymbol{\sigma}_o^{-1} \cdot \mathscr{P} \boldsymbol{V}_{Jo} - \boldsymbol{E}_{\mathrm{E}}). \tag{19}$$

Subtracting Equation (19) from (18) yields ($\delta \boldsymbol{\sigma}^{-1} \stackrel{\mathrm{def}}{=} \boldsymbol{\sigma}^{-1} - \boldsymbol{\sigma}_o^{-1}$)

$$\boldsymbol{s}_{\mathrm{J}} - \boldsymbol{s}_{Jo} = \frac{\mathscr{P}}{E_o} (\boldsymbol{\sigma}_o^{-1} \cdot (\boldsymbol{V}_{\mathrm{J}} - \boldsymbol{V}_{Jo}) + \delta \boldsymbol{\sigma}^{-1} \cdot \boldsymbol{V}_{\mathrm{J}}). \tag{20}$$

Taking the norms of both sides, and using the Cauchy–Schwarz and Triangle inequalities, as well as the representations, $\boldsymbol{V}_{\mathrm{J}} = \|\boldsymbol{V}_{\mathrm{J}}\| \boldsymbol{s}_{\mathrm{J}}$ and $\boldsymbol{V}_{Jo} = \|\boldsymbol{V}_{Jo}\| \boldsymbol{s}_{Jo}$ yields

$$\begin{aligned}
\|\boldsymbol{s}_{\mathrm{J}} - \boldsymbol{s}_{Jo}\| &= \| \frac{\mathscr{P}}{E_o} (\boldsymbol{\sigma}_o^{-1} \cdot (\boldsymbol{V}_{\mathrm{J}} - \boldsymbol{V}_{Jo}) + \delta \boldsymbol{\sigma}^{-1} \cdot \boldsymbol{V}_{\mathrm{J}}) \| \\
&\leqslant \frac{|\mathscr{P}|}{|E_o|} (\|\boldsymbol{\sigma}_o^{-1}\| \|\boldsymbol{V}_{\mathrm{J}} - \boldsymbol{V}_{Jo}\| + \|\delta \boldsymbol{\sigma}^{-1}\| \|\boldsymbol{V}_{\mathrm{J}}\|) \\
&\leqslant \frac{|\mathscr{P}|}{|E_o|} (\|\boldsymbol{\sigma}_o^{-1}\| (\|\|\boldsymbol{V}_{\mathrm{J}}\| \boldsymbol{s}_{\mathrm{J}} - \|\boldsymbol{V}_{Jo}\| \boldsymbol{s}_{Jo}\|) + \|\delta \boldsymbol{\sigma}^{-1}\| \|\boldsymbol{V}_{\mathrm{J}}\|) \\
&\leqslant \frac{|\mathscr{P}| \, \|\boldsymbol{V}_{\mathrm{J}}\|}{|E_o|} \left(\|\boldsymbol{\sigma}_o^{-1}\| \left(\left\| \boldsymbol{s}_{\mathrm{J}} - \frac{\|\boldsymbol{V}_{Jo}\|}{\|\boldsymbol{V}_{\mathrm{J}}\|} \boldsymbol{s}_{Jo} \right\| \right) + \|\delta \boldsymbol{\sigma}^{-1}\| \right).
\end{aligned} \tag{21}$$

If we assume that the *magnitudes* of the velocities in both cases are the same, $\|\boldsymbol{V}_{\mathrm{J}}\| = \|\boldsymbol{V}_{Jo}\|$ (this may not necessarily be true, in general), we obtain

$$\|\boldsymbol{s}_{\mathrm{J}} - \boldsymbol{s}_{Jo}\| \leqslant \frac{|\mathscr{P}| \, \|\boldsymbol{V}_{\mathrm{J}}\|}{|E_o|} (\|\boldsymbol{\sigma}_o^{-1}\| \|\boldsymbol{s}_{\mathrm{J}} - \boldsymbol{s}_{Jo}\| + \|\delta \boldsymbol{\sigma}^{-1}\|), \tag{22}$$

and one has

$$\|\boldsymbol{s}_{\mathrm{J}} - \boldsymbol{s}_{Jo}\| \leqslant \frac{b}{1-a} = \frac{\frac{|\mathscr{P}|}{|E_o|} \|\boldsymbol{V}_{\mathrm{J}}\| \|\delta \boldsymbol{\sigma}^{-1}\|}{1 - \frac{|\mathscr{P}|}{|E_o|} \|\boldsymbol{V}_{\mathrm{J}}\| \|\boldsymbol{\sigma}_o^{-1}\|} = \frac{\|\delta \boldsymbol{\sigma}^{-1}\|}{\frac{|E_o|}{|\mathscr{P}| \, \|\boldsymbol{V}_{\mathrm{J}}\|} - \|\boldsymbol{\sigma}_o^{-1}\|}, \tag{23}$$

provided that $a < 1$, where $a \stackrel{\mathrm{def}}{=} |\mathscr{P}| \, \|\boldsymbol{V}_{\mathrm{J}}\| \|\boldsymbol{\sigma}_o^{-1}\| / |E_o|$ and $b \stackrel{\mathrm{def}}{=} |\mathscr{P}| \, \|\boldsymbol{V}_{\mathrm{J}}\| \|\delta \boldsymbol{\sigma}^{-1}\| / |E_o|$. We have the following key observations:

- Increasing the anisotropic conductivity perturbation ($\delta \boldsymbol{\sigma}$) magnitude will increase the difference in trajectories ($\|\delta \boldsymbol{\sigma}\| \propto \|\delta \boldsymbol{\sigma}^{-1}\|$).
- Increasing the isotropic base conductivity ($\boldsymbol{\sigma}_o^{-1}$) magnitude will increase the difference in trajectories.

DOI: 10.1002/nme

- Increasing the jet's inherent electric field strength ($|E_o|$) decreases the difference in trajectories.
- Increasing the jet's inherent charge ($|\mathscr{P}|$) increases the difference in trajectories.
- Increasing the jet's velocity magnitude ($\|\boldsymbol{V}_\mathrm{J}\|$) increases the difference in trajectories.

The above results provide qualitative characterization of the deviation in the trajectory due to anisotropic effects. However, quantitative differences need to be dealt with numerically, which we discuss next.

Remark
The splitting (bifurcation, trifurcation, etc) of currents, sometimes observed in lightning bolts, can be accounted for by considering a non-linear constitutive law (replacing the linear relation in Equation (1)) relating the current to the electrical field, for example of the form

$$\boldsymbol{J}=\mathscr{P}\boldsymbol{V}=\mathscr{F}(\boldsymbol{E}). \tag{24}$$

This would allow for, in addition to the direction changes due to anisotropic perturbations, current splits. In the particular case of lightning, since it propagates in 'steps', with very brief pauses, it attracts stray currents/charges from the ground and surrounding atmosphere leading to the observed bolt splitting. This is beyond the scope of the present work. For detailed discussions on lightning-specific phenomena, see Rakov and Uman [7], Demirkol *et al.* [8], Uman [9], Fishman *et al.* [10], Inan *et al.* [11] and Inan and Inan [2].

5. NUMERICAL METHODS

Consider the expression relating the position of the electrical jet tip and its velocity

$$\dot{\boldsymbol{r}}_\mathrm{J}=\boldsymbol{V}_\mathrm{J}(\boldsymbol{r}_\mathrm{J}). \tag{25}$$

Expanding $\boldsymbol{r}_\mathrm{J}$ in a Taylor series about $t+\phi\Delta t$, where $0\leqslant\phi\leqslant1$, we obtain

$$\boldsymbol{r}_\mathrm{J}(t+\Delta t)=\boldsymbol{r}_\mathrm{J}(t+\phi\Delta t)+\dot{\boldsymbol{r}}_\mathrm{J}|_{t+\phi\Delta t}(1-\phi)\Delta t+\tfrac{1}{2}\ddot{\boldsymbol{r}}_\mathrm{J}|_{t+\phi\Delta t}(1-\phi)^2(\Delta t)^2+\mathscr{O}(\Delta t)^3, \tag{26}$$

and

$$\boldsymbol{r}_\mathrm{J}(t)=\boldsymbol{r}_\mathrm{J}(t+\phi\Delta t)-\dot{\boldsymbol{r}}_\mathrm{J}|_{t+\phi\Delta t}\phi\Delta t+\tfrac{1}{2}\ddot{\boldsymbol{r}}_\mathrm{J}|_{t+\phi\Delta t}\phi^2(\Delta t)^2+\mathscr{O}(\Delta t)^3. \tag{27}$$

Subtracting the two expressions yields

$$\dot{\boldsymbol{r}}_\mathrm{J}|_{t+\phi\Delta t}=\frac{\boldsymbol{r}_\mathrm{J}(t+\Delta t)-\boldsymbol{r}_\mathrm{J}(t)}{\Delta t}+\hat{\mathscr{O}}(\Delta t), \tag{28}$$

where $\hat{\mathscr{O}}(\Delta t)=\mathscr{O}(\Delta t)^2$ when $\phi=\frac{1}{2}$, and $\hat{\mathscr{O}}(\Delta t)=\mathscr{O}(\Delta t)$ when $\phi\neq\frac{1}{2}$. Inserting this into the governing equations yields

$$\boldsymbol{r}_\mathrm{J}(t+\Delta t)=\boldsymbol{r}_\mathrm{J}(t)+\Delta t\boldsymbol{V}_\mathrm{J}(t+\phi\Delta t)+\hat{\mathscr{O}}(\Delta t)^2. \tag{29}$$

The term $\boldsymbol{V}_\mathrm{J}(t+\phi\Delta t)$ can be computed via a 'trapezoidal' approximation

$$\boldsymbol{V}_\mathrm{J}(t+\phi\Delta t)\approx\phi\boldsymbol{V}_\mathrm{J}(\boldsymbol{r}_\mathrm{J}(t+\Delta t))+(1-\phi)\boldsymbol{V}_\mathrm{J}(\boldsymbol{r}_\mathrm{J}(t)), \tag{30}$$

DOI: 10.1002/nme

yielding

$$\begin{aligned}\boldsymbol{r}_{\mathrm{J}}(t+\Delta t) &= \boldsymbol{r}_{\mathrm{J}}(t)+\Delta t\boldsymbol{V}_{\mathrm{J}}(t+\phi\Delta t)+\hat{\mathscr{O}}(\Delta t)^2 \\ &= \boldsymbol{r}_{\mathrm{J}}(t)+\Delta t(\phi\boldsymbol{V}_{\mathrm{J}}(\boldsymbol{r}_{\mathrm{J}}(t+\Delta t))+(1-\phi)\boldsymbol{V}_{\mathrm{J}}(\boldsymbol{r}_{\mathrm{J}}(t)))+\hat{\mathscr{O}}(\Delta t)^2. \end{aligned} \tag{31}$$

We note that (1) when $\phi=1$, this collapses to the (implicit) Backward Euler scheme, which is very stable (very dissipative) and $\mathscr{O}(\Delta t)^2$ locally in time, (2) when $\phi=0$, this collapses to the (explicit) Forward Euler scheme, which is conditionally stable and $\mathscr{O}(\Delta t)^2$ locally in time and (3) when $\phi=0.5$, this collapses to the (implicit) Midpoint scheme, which is marginally stable and $\hat{\mathscr{O}}(\Delta t)^2=\mathscr{O}(\Delta t)^3$ locally in time.

5.1. Application to the charged jet

The position vector of the jet can be integrated via a, ϕ-rule**

$$\boldsymbol{r}_{\mathrm{J}}(t+\Delta t)=\boldsymbol{r}_{\mathrm{J}}(t)+\Delta t(\phi\boldsymbol{V}_{\mathrm{J}}(t+\Delta t)+(1-\phi)\boldsymbol{V}_{\mathrm{J}}(t)), \tag{32}$$

which is coupled to

$$\boldsymbol{V}_{\mathrm{J}}=\frac{1}{\mathscr{P}}\boldsymbol{\sigma}\cdot(\boldsymbol{E}_{\mathrm{J}}+\boldsymbol{E}_{\mathrm{E}}). \tag{33}$$

This leads to a coupled set of non-linear equations which can be solved in an adaptive iterative manner.

5.2. Iterative solution methods

Implicit time-stepping methods, with time step size adaptivity, built on approaches found in Zohdi [45–50], will be used throughout the upcoming analysis, which starts by discretizing the equations of jet motion $\dot{\boldsymbol{r}}_{\mathrm{J}}=\boldsymbol{V}_{\mathrm{J}}$ using a ϕ-method (L denotes the time step)

$$\boldsymbol{r}_{\mathrm{J}}^{L+1}=\boldsymbol{r}_{\mathrm{J}}^{L}(t)+\Delta t(\phi\boldsymbol{V}_{\mathrm{J}}^{L+1}+(1-\phi)\boldsymbol{V}_{\mathrm{J}}^{L}), \tag{34}$$

one arrives at the following abstract form

$$\mathscr{A}(\boldsymbol{r}_{\mathrm{J}}^{L+1})=\mathscr{B}. \tag{35}$$

It is convenient to write

$$\mathscr{A}(\boldsymbol{r}_{\mathrm{J}}^{L+1})-\mathscr{B}=\mathscr{G}(\boldsymbol{r}_{\mathrm{J}}^{L+1})-\boldsymbol{r}_{\mathrm{J}}^{L+1}+\mathscr{R}=\boldsymbol{0}, \tag{36}$$

where $\mathscr{R}$ is a remainder term that does not depend on the solution, i.e.

$$\mathscr{R}\neq\mathscr{R}(\boldsymbol{r}_{\mathrm{J}}^{L+1}). \tag{37}$$

A straightforward iterative scheme can be written as

$$\boldsymbol{r}_{\mathrm{J}}^{L+1,K}=\mathscr{G}(\boldsymbol{r}_{\mathrm{J}}^{L+1,K-1})+\mathscr{R}, \tag{38}$$

**In order to streamline the notation, we drop the cumbersome $\mathscr{O}(\Delta t)$-type terms.

DOI: 10.1002/nme

where $K=1,2,3,\ldots$ is the index of iteration within time step $L+1$. The convergence of such a scheme is dependent on the behavior of $\mathscr{G}$. Namely, a sufficient condition for convergence is that $\mathscr{G}$ is a contraction mapping for all $\boldsymbol{r}_{\mathrm{J}}^{L+1,K}$, $K=1,2,3\ldots$ In order to investigate this further, we define the iteration error as

$$\varpi^{L+1,K} \stackrel{\text{def}}{=} \boldsymbol{r}_{\mathrm{J}}^{L+1,K} - \boldsymbol{r}_{\mathrm{J}}^{L+1}. \tag{39}$$

A necessary restriction for convergence is iterative self consistency, i.e. the 'exact' (discretized) solution must be represented by the scheme

$$\mathscr{G}(\boldsymbol{r}_{\mathrm{J}}^{L+1}) + \mathscr{R} = \boldsymbol{r}_{\mathrm{J}}^{L+1}. \tag{40}$$

Enforcing this restriction, a sufficient condition for convergence is the existence of a contraction mapping

$$\begin{aligned} \varpi^{L+1,K} = \|\boldsymbol{r}_{\mathrm{J}}^{L+1,K} - \boldsymbol{r}_{\mathrm{J}}^{L+1}\| &= \|\mathscr{G}(\boldsymbol{r}_{\mathrm{J}}^{L+1,K-1}) - \mathscr{G}(\boldsymbol{r}_{\mathrm{J}}^{L+1})\| \\ &\leqslant \eta^{L+1,K}\|\boldsymbol{r}_{\mathrm{J}}^{L+1,K-1} - \boldsymbol{r}_{\mathrm{J}}^{L+1}\|, \end{aligned} \tag{41}$$

where, if $0 \leqslant \eta^{L+1,K} < 1$ for each iteration K, then $\varpi^{L+1,K} \to \mathbf{0}$ for any arbitrary starting value $\boldsymbol{r}_{\mathrm{J}}^{L+1,K=0}$, as $K \to \infty$. This type of contraction condition is sufficient, but not necessary, for convergence. Inserting this into $\dot{\boldsymbol{r}}_{\mathrm{J}} = \boldsymbol{V}_{\mathrm{J}}(\boldsymbol{r}_{\mathrm{J}})$ leads to

$$\boldsymbol{r}_{\mathrm{J}}^{L+1,K} = \underbrace{\phi \Delta t \boldsymbol{V}_{\mathrm{J}}(\boldsymbol{r}_{\mathrm{J}}^{L+1,K-1})}_{\mathscr{G}} + \underbrace{\boldsymbol{r}_{\mathrm{J}}^{L} + \Delta t((1-\phi)\boldsymbol{V}_{\mathrm{J}}(\boldsymbol{r}_{\mathrm{J}}^{L}))}_{\mathscr{R}}, \tag{42}$$

whose convergence is controlled largely by the multiplier $\eta \propto \Delta t$ and the magnitude of the jet velocity. Therefore, if convergence is slow within a time step, the time step size, which is adjustable, can be reduced by an appropriate amount to increase the rate of convergence. Thus, decreasing the time step size improves the convergence; however, we want to simultaneously maximize the time-step sizes to decrease the overall computing time, while still meeting an error tolerance on the numerical solution's accuracy. In order to achieve this goal, we follow an approach found in Zohdi [45–50] originally developed for continuum thermo-chemical multifield problems in which (1) one approximates the contraction constant as $\eta^{L+1,K} \approx S(\Delta t)^p$, S being a constant and (2) one assumes that the error within an iteration behaves according to $(S(\Delta t)^p)^K \varpi^{L+1,0} = \varpi^{L+1,K}$, where $K=1,2,\ldots$, where $\varpi^{L+1,0}$ is the initial norm of the iterative error and S is intrinsic to the system.[††] Our goal is to meet an error tolerance in exactly a preset number of iterations. To this end, one writes $(S(\Delta t_{\mathrm{tol}})^p)^{K_d} \varpi^{L+1,0} = \mathrm{TOL}$, where TOL is a tolerance and where K_d is the number of desired iterations. Typically, K_d is chosen to be between five to ten iterations. If the error tolerance is not met in the desired number of iterations, the contraction constant $\eta^{L+1,K}$ is too large. Accordingly, one can solve for a new smaller step size, under the assumption that S is

[††]For the class of problems under consideration, due to the quasilinear dependency or Δt, $p \approx 1$.

DOI: 10.1002/nme

constant,

$$\Delta t_{\text{tol}} = \Delta t \left(\frac{\left(\frac{\text{TOL}}{\varpi^{L+1,0}} \right)^{1/pK_d}}{\left(\frac{\varpi^{L+1,K}}{\varpi^{L+1,0}} \right)^{1/pK}} \right). \tag{43}$$

The assumption that S is constant is not critical, since the time steps are to be recursively refined and unrefined throughout the simulation. Clearly, the expression in Equation (43) can also be used for time step enlargement, if convergence is met in less than K_d iterations. An implementation of the procedure is as follows:

ITERATIVE PROCESS: (*INITIALLY SET* $K=0$):

(1) COMPUTE VELOCITY:

$$\boldsymbol{V}_{\text{J}}^{K+1}(t+\Delta t) = \frac{1}{\mathcal{P}} \boldsymbol{\sigma} \cdot (\boldsymbol{E}_{\text{J}}^{K}(t+\Delta t) + \boldsymbol{E}_{E}^{K}(t+\Delta t))$$

(2) COMPUTE POSITION:

$$\boldsymbol{r}_{\text{J}}^{K+1}(t+\Delta t) = \boldsymbol{r}_{\text{J}}(t) + \Delta t (\phi \boldsymbol{V}_{\text{J}}^{K+1}(t+\Delta t) + (1-\phi)\boldsymbol{V}_{\text{J}}(t))$$

(3) COMPUTE ELECTRIC FIELD CONTRIBUTION CORRECTIONS:

$$\boldsymbol{E}_{\text{J}}^{K+1}(t+\Delta t) = E_o \frac{\boldsymbol{V}_{\text{J}}^{K+1}(t+\Delta t)}{\|\boldsymbol{V}_{\text{J}}^{K+1}(t+\Delta t)\|}$$

$$\boldsymbol{E}_{\text{E}}^{K+1}(t+\Delta t) = \mathscr{F}(\boldsymbol{r}_{\text{J}}^{K+1}(t+\Delta t), \boldsymbol{r}_{\text{E}})$$

(4) COMPUTE ERROR MEASURES:

$$(a)\, \varpi_K \stackrel{\text{def}}{=} \frac{\|\boldsymbol{r}_{\text{J}}^{K+1}(t+\Delta t) - \boldsymbol{r}_{\text{J}}^{K}(t+\Delta t)\|}{\|\boldsymbol{r}_{\text{J}}^{K+1}(t+\Delta t) - \boldsymbol{r}_{\text{J}}(t)\|} \qquad \text{(normalized)}$$

$$(b)\, Z_K \stackrel{\text{def}}{=} \frac{\varpi_K}{\text{TOL}_r}$$

$$(c)\, \Phi_K \stackrel{\text{def}}{=} \left(\frac{(\frac{\text{TOL}}{\varpi_0})^{\frac{1}{pK_d}}}{(\frac{\varpi_K}{\varpi_0})^{\frac{1}{pK}}} \right)$$

CHECK: IF TOLERANCE MET ($Z_K \leqslant 1$) AND $K < K_d$ THEN:

(*a*) INCREMENT TIME: $t = t + \Delta t$

(*b*) CONSTRUCT NEW TIME STEP: $\Delta t = \Phi_K \Delta t$

(*c*) SELECT MINIMUM: $\Delta t = \text{MIN}(\Delta t^{\text{lim}}, \Delta t)$ AND GO TO (1)

CHECK: IF TOLERANCE NOT MET ($Z_K > 1$) AND $K = K_d$ THEN:

(*a*) CONSTRUCT NEW TIME STEP: $\Delta t = \Phi_K \Delta t$

(*b*) RESTART AT TIME = t AND GO TO (1)

(44)

DOI: 10.1002/nme

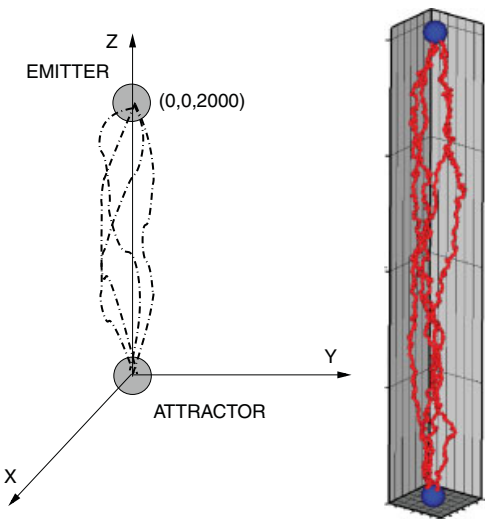

Figure 3. Left: The model problem (showing multiple current jets). Right: Four numerical realizations for the same starting conditions for a current jet trajectory for $\delta\sigma/\sigma_o = 0.5$; see the separated frames in Figure 4.

6. A MODEL PROBLEM

A series of numerical experiments (Figure 3) were performed where the magnitude of anisotropic perturbations was steadily increased, and the variability of the path length taken by the current was measured (the average and standard deviation). For the model problem under consideration, we employ a simple external electric field[‡‡]

$$\boldsymbol{E}_{\mathrm{E}} = \mathscr{F}(\boldsymbol{r}_{\mathrm{J}}, \boldsymbol{r}_{\mathrm{E}}) = c_1 \mathrm{e}^{c_2 \|\boldsymbol{r}_{\mathrm{E}} - \boldsymbol{r}_{\mathrm{J}}\|} \boldsymbol{s}_{J \to E}, \tag{45}$$

where $\boldsymbol{s}_{J \to E}$ is the unit vector pointing from the free-surface front toward the external source. For each parameter set, 100 jets (Figures 3 and 4) were computed with the same starting conditions, but with different random atmospheres. The system parameters were[§§]

- The starting location of the jet: $\boldsymbol{r}_{\mathrm{J}} = (0, 0, 2000)$.
- The attractor's location: $\boldsymbol{r}_{\mathrm{E}} = (0, 0, 0)$.
- The external field constants: $c_1 = 10^6$ and $c_2 = -0.0001$.
- The jet charge (per unit volume), $\mathscr{P} = 0.01$.
- The initial velocity of the jet $\boldsymbol{V}_{\mathrm{J}}(t=0) = (0, 0, -200000)$.
- The initial time-step $\Delta t(t=0) = 1/\|\boldsymbol{V}_{\mathrm{J}}(t=0)\|$.

[‡‡]One can find realistic electrical field distributions for atmospheric variations in Volland [51], Markson [52], MacGorman and Rust [53], Uman [54] and Rakov and Uman [7]. One could also include an increase in conductivity with height (z), which is somewhat standard in atmospheric sciences (Rakov and Uman [7]), although this was not incorporated in the present model problem.

[§§]Localized atmospheric electrical emissions, such as lightning, travel at between 2×10^5 m/s $- 10^6$ m/s. The average current is approximate 100–200 A. The peak current is approximately 1000–2000 A. As a comparison, consider that a light bulb operates at 1 A and an electrical socket at 15 A.

DOI: 10.1002/nme

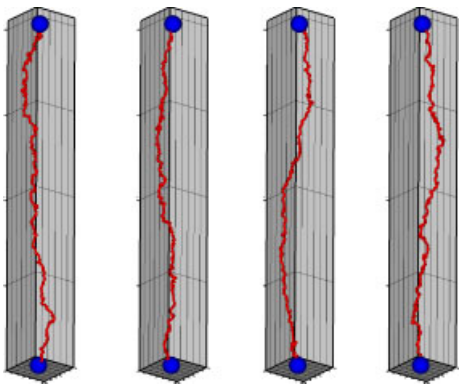

Figure 4. Various numerical realizations for the same starting conditions for a current jet trajectory.

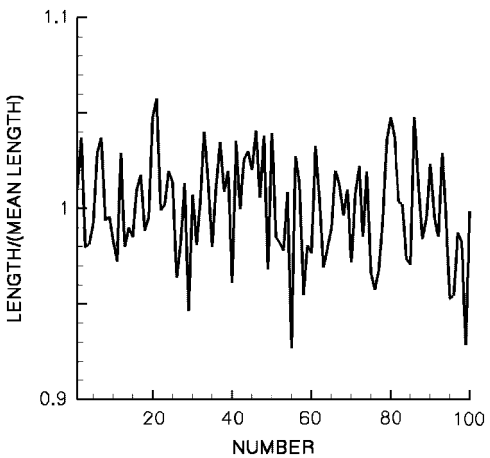

Figure 5. Typical scatter (normalized path length, $\mathscr{L}$) for 100 jets $\delta\sigma/\sigma_o = 0.3$.

- The value of the jet-electric field contribution is $E_o = \mathscr{P}\|\boldsymbol{V}_{\mathrm{J}}(t=0)\|/\sigma_o$.

We describe the jet behavior statistically by post-processing the data in Figure 5, specifically computing the average ($\mathscr{A}$)

$$\mathscr{A} \stackrel{\text{def}}{=} \frac{1}{N}\sum_{i=1}^{N} L_i, \tag{46}$$

and standard deviation ($\mathscr{S}$)

$$\mathscr{S} \stackrel{\text{def}}{=} \sqrt{\frac{1}{N}\sum_{i=1}^{N}(L_i - \mathscr{A})^2}. \tag{47}$$

DOI: 10.1002/nme

We also tracked the ratio of the average path traveled by the anisotropically perturbed path to the isotropic 'base state' path (L^*), defined by $\mathscr{L} = \mathscr{A}/L^*$. The total normalized path 'length' of the current path was curve-fit versus the degree of anisotropy, $\theta \stackrel{\text{def}}{=} \delta\sigma/\sigma_o$ yielding

$$\mathscr{L} = c\theta + d \Rightarrow \mathscr{L} = 2.9459\theta + 0.8152, \tag{48}$$

with an error of

$$\sqrt{\frac{\sum (c\theta_i + d - \mathscr{L}_i)^2}{\sum \mathscr{L}_i^2}} = 0.01003, \tag{49}$$

where L_i is the length traveled by the ith jet. The extremely high quality of the fit should not be that surprising, since the relation derived earlier (Equation (23)), although under some addition assumptions, suggests that

$$\|\boldsymbol{s}_{\mathrm{J}} - \boldsymbol{s}_{\mathrm{J}o}\| \leqslant \frac{\|\delta\boldsymbol{\sigma}^{-1}\|}{\dfrac{|E_o|}{|\mathscr{P}|\|\boldsymbol{V}_{\mathrm{J}}\|} - \|\boldsymbol{\sigma}_o^{-1}\|} \propto \|\delta\boldsymbol{\sigma}^{-1}\|. \tag{50}$$

and where $\|\delta\boldsymbol{\sigma}\| \propto \|\delta\boldsymbol{\sigma}^{-1}\|$.

As the trajectories are bounded by a constant, clearly the distance traveled would be well approximated by a lower-order function of the degree of perturbation, for example a linear or quasilinear function of that same variable, provided that the current is drawn to the object, as in the discussed example.

Remark

Another possible measure of the characteristics of the jets is the excursion ($\mathscr{E}$) away from the z-axis, described by

$$\mathscr{E} \stackrel{\text{def}}{=} \frac{1}{L_o} \max_{\text{jets}} \sqrt{r_x^2 + r_y^2}, \tag{51}$$

where r_x and r_y are the maximum deviations in the x and y directions from the vertical (z-axis). The excursion provides the ratio of the minor axis (lateral displacement) and major axis of an 'envelope cylinder' (longitudinal displacement) that contains all trajectories of the jets. The column on the far right of Table I provides information about the excursion's dependence on the perturbation magnitude, and is similar in character to the previous measure described by Equation (49).

Table I. The statistics as a function of perturbation magnitude (100 jets) for $c_2 = -0.0001$.

$\delta\sigma/\sigma_o$	$\mathscr{L}$	$\mathscr{A}$	$\mathscr{S}$	$\mathscr{E}$
0.1000	1.1339	2267.8677	11.0461	0.0373
0.2000	1.3836	2767.3374	48.9579	0.0597
0.3000	1.6855	3371.1999	91.6825	0.0723
0.4000	1.9866	3973.2473	167.8376	0.0874
0.5000	2.3054	4610.9718	248.0099	0.0969

DOI: 10.1002/nme

7. CONCLUSIONS

A model for the trajectory of localized electrical current flow in anisotropically perturbed atmospheres was developed. Relevant applications span natural phenomena, such as lightning and industrial ignition systems, which are employed in combustion cycles. The approach was to relate the charge carrier velocity to the local anisotropy of the atmospheric conductivity, leading to a system of non-linear equations for the trajectory of the electrical current path. A qualitative analysis was performed to determine the dependence of the trajectory of the current as a function of the degree of anisotropy. Quantitative statistical results were achieved numerically using an adaptive implicit temporally adaptive time-stepping scheme. The analysis provides insight into what system features qualitatively and quantitatively control the paths taken by electrical currents in gaseous atmospheres. For a more detailed analysis, the simulation of charged particulate plasma streams/jets (which comprise the currents) is critical. Such calculations are computationally intensive. Until recently, the detailed simulation of such jets has been computationally intractable. However, within the last decade, simultaneous advances in computational methods, applied mathematics and high performance computing have raised the possibility that an analyst can directly simulate an engineering scale device being impacted by charged jets containing billions or even trillions of particles, incorporating all of the important microscale details. It is important to note, as mentioned at the outset of this paper, that charged particulate jets also have relevance to the analysis and control of charged ion plasmas in combustion chambers. Modeling and numerical solution strategies to analyze the coupled thermal, mechanical and electromagnetic response of such charged particulate jets, and random particulate systems in general, have been extensively studied in Zohdi [45–50, 55], and are a topic of current investigation by the author.

APPENDIX A: CONDUCTIVE MATERIAL SYMMETRY

In order to determine one plane of conductive symmetry, consider the following:

- STEP 1: Reflect the x_1 axis

$$\boldsymbol{R}(x_1)\cdot\boldsymbol{x} \stackrel{\text{def}}{=} \begin{bmatrix} -1 & 0 & 0 \\ 0 & 1 & 0 \\ 0 & 0 & 1 \end{bmatrix} \begin{Bmatrix} x_1 \\ x_2 \\ x_3 \end{Bmatrix} = \begin{Bmatrix} \hat{x}_1 \\ \hat{x}_2 \\ \hat{x}_3 \end{Bmatrix} = \begin{Bmatrix} -x_1 \\ x_2 \\ x_3 \end{Bmatrix}. \tag{A1}$$

- STEP 2:Transform the $\boldsymbol{E}$ and $\boldsymbol{J}$ vectors with the same transformation,

$$\boldsymbol{R}(x_1)\cdot\boldsymbol{E} \stackrel{\text{def}}{=} \begin{bmatrix} -1 & 0 & 0 \\ 0 & 1 & 0 \\ 0 & 0 & 1 \end{bmatrix} \begin{Bmatrix} E_1 \\ E_2 \\ E_3 \end{Bmatrix} = \begin{Bmatrix} \hat{E}_1 \\ \hat{E}_2 \\ \hat{E}_3 \end{Bmatrix} = \begin{Bmatrix} -E_1 \\ E_2 \\ E_3 \end{Bmatrix}. \tag{A2}$$

DOI: 10.1002/nme

and

$$\boldsymbol{R}(x_1)\cdot\boldsymbol{J}\overset{\text{def}}{=}\begin{bmatrix}-1 & 0 & 0\\ 0 & 1 & 0\\ 0 & 0 & 1\end{bmatrix}\begin{Bmatrix}J_1\\ J_2\\ J_3\end{Bmatrix}=\begin{Bmatrix}\hat{J}_1\\ \hat{J}_2\\ \hat{J}_3\end{Bmatrix}=\begin{Bmatrix}-J_1\\ J_2\\ J_3\end{Bmatrix}. \tag{A3}$$

- STEP 3: Transform the $\boldsymbol{\sigma}$ with the same transformation, but for second order tensor rules:

$$\begin{bmatrix}-1 & 0 & 0\\ 0 & 1 & 0\\ 0 & 0 & 1\end{bmatrix}\begin{bmatrix}\sigma_{11} & \sigma_{12} & \sigma_{13}\\ \sigma_{21} & \sigma_{22} & \sigma_{23}\\ \sigma_{31} & \sigma_{32} & \sigma_{33}\end{bmatrix}\begin{bmatrix}-1 & 0 & 0\\ 0 & 1 & 0\\ 0 & 0 & 1\end{bmatrix}=\begin{bmatrix}\hat{\sigma}_{11} & \hat{\sigma}_{12} & \hat{\sigma}_{13}\\ \hat{\sigma}_{21} & \hat{\sigma}_{22} & \hat{\sigma}_{23}\\ \hat{\sigma}_{31} & \hat{\sigma}_{32} & \hat{\sigma}_{33}\end{bmatrix}, \tag{A4}$$

and thus

$$\begin{bmatrix}\hat{\sigma}_{11} & \hat{\sigma}_{12} & \hat{\sigma}_{13}\\ \hat{\sigma}_{21} & \hat{\sigma}_{22} & \hat{\sigma}_{23}\\ \hat{\sigma}_{31} & \hat{\sigma}_{32} & \hat{\sigma}_{33}\end{bmatrix}=\begin{bmatrix}\sigma_{11} & -\sigma_{12} & -\sigma_{13}\\ -\sigma_{21} & \sigma_{22} & \sigma_{23}\\ -\sigma_{31} & \sigma_{32} & \sigma_{33}\end{bmatrix}. \tag{A5}$$

- STEP 4: All components that are not equal before and after the reflection of axes are zero:

$$\begin{Bmatrix}\hat{J}_1\\ \hat{J}_2\\ \hat{J}_3\end{Bmatrix}=\begin{bmatrix}\sigma_{11} & 0 & 0\\ 0 & \sigma_{22} & \sigma_{23}\\ 0 & \sigma_{32} & \sigma_{33}\end{bmatrix}\begin{Bmatrix}\hat{E}_1\\ \hat{E}_2\\ \hat{E}_3\end{Bmatrix}. \tag{A6}$$

The end result is a 'Monoclinic' medium, i.e. one plane of electrical symmetry (x_2-x_3 plane)(4 free constants)

$$\boldsymbol{\sigma}\overset{\text{def}}{=}\begin{bmatrix}\sigma_{11} & 0 & 0\\ 0 & \sigma_{22} & \sigma_{23}\\ 0 & \sigma_{32} & \sigma_{33}\end{bmatrix}. \tag{A7}$$

Repeating the procedure for a symmetry about the x_1-x_3 plane yields

$$\boldsymbol{\sigma}\overset{\text{def}}{=}\begin{bmatrix}\sigma_{11} & 0 & 0\\ 0 & \sigma_{22} & 0\\ 0 & 0 & \sigma_{33}\end{bmatrix}. \tag{A8}$$

Repeating the procedure for a symmetry about the x_1-x_2 changes nothing. Performing rotations about the x_3-axis yields $\sigma_{22}=\sigma_{33}$ and performing rotations about the x_2-axis yields $\sigma_{11}=\sigma_{33}$, thus yielding

$$\boldsymbol{\sigma}\overset{\text{def}}{=}\begin{bmatrix}\sigma & 0 & 0\\ 0 & \sigma & 0\\ 0 & 0 & \sigma\end{bmatrix}. \tag{A9}$$

DOI: 10.1002/nme

$\sigma_{11} = \sigma_{22} = \sigma_{33} = \sigma$. This immediately implies that there are an infinite number of planes where the material properties are equal in all directions, and thus a single-material constant. The medium is of the familiar *isotropic* variety. An isotropic medium has material properties that are the same in every direction at a point in the medium, i.e. the properties are not a function of orientation at a point in the medium.

REFERENCES

1. Townsend JS. *Electricity in Gases*. Oxford University Press: Oxford, 1914.
2. Inan US, Inan A. *Engineering Electromagnetics*. Addison-Wesley: Reading, MA, 1999.
3. Bering EA, Rosenberg TJ, Benbrook JR, Detrick D, Matthews DL, Rycroft MJ, Saunders MA, Sheldon WR. Electrical fields, electron precipitation, and VLF radiation during a simultaneous magnetospheric substorm and atomospheric thunderstorm. *Journal of Geophysical Research* 1980; **85**:55–72.
4. Holzworth RH, Norville KW, Kintner PM, Power SP. Stratospheric conductivity variations over thunderstorms. *Journal of Geophysical Research* 1986; **93**:3915–3917.
5. Pinto IRCA, Pinto O, Gonzalez WD, Dutra LG, Wygant J, Mozer FS. Stratospheric electric field and conductivity measurements over electrified convective clouds in the South American region. *Journal of Geophysical Research* 1988; **93**:709–715.
6. Hu H, Holzworth RH, Li YQ. Thunderstorm related variations in stratospheric conductivity measurements. *Journal of Geophysical Research* 1989; **94**(16):429–435.
7. Rakov V, Uman M. *Lightning*: *Physics and Effects*. Cambridge University Press: Cambridge, 2003.
8. Demirkol MK, Inan US, Bell TF, Kanekal SG, Wilkinson DC. Ionospheric effects of relativistic electron enhancement events. *Geophysical Research Letters* 1999; **26**(23):3557–3560.
9. Uman MA. *All About Lightning*. Dover: New York, 1986; 103–110.
10. Fishman GJ, Bhat PN, Malozzi R, Horack JM, Koshut T, Kouvelioton C, Pendleton GN, Meegan CA, Wilson RB, Paciesas WS, Goodman SJ, Christian HJ. Discovery of intense gamma-ray flashes of atmospheric origin. *Science* 1994; **264**:1313–1316.
11. Inan US, Reising SC, Fishman GJ, Horack JM. On the association of terrestrial gamma-ray bursts with lightning and implications for sprites. *Geophysical Research Letters* 1996; **23**(9):1017–1020.
12. Azevedo RG, Jones DG, Jog AV, Jamshidi B, Myers DR, Chen L, Fu X-A, Mehregany M, Wijesundara MBJ, Pisano AP. A SiC MEMS resonant strain sensor for harsh environment applications. *IEEE Sensors Journal* 2007; **7**(4):568–576.
13. Schwartz SW, Myers DR, Kramer RK, Choi S, Jordan A, Wijesundara MBJ, Hopcroft MA, Pisano AP. Silicon and Silicon Carbide Survivability in an In-Cylinder Combustion Environment. *PowerMEMS 2008*, Sendai, Japan, 9–12 November 2008.
14. Ikeda Y, Nishiyama A, Kaneko M. Microwave enhanced ignition process for fuel mixture at elevated pressure of 1 MPa. *47th AIAA Aerospace Sciences Meeting Including the New Horizons Forum and Aerospace Exposition* 5–8 January 2009, Orlando, FL, 2009.
15. Kaneko M, Nishiyama A, Jeong H, Kantano H, Ikeda I. *Combustion Characteristics of Microwave Plasma Combustion Engine*. Japanese Society of Automotive Engineers: Tokyo, Japan, May 2008; 7–11.
16. Leipold F, Stark RH, El-Habachi A, Schoenbach KH. Electron density measurements in an atmospheric pressure air plasma by means of IR heterodyne interferometry. *Journal of Physics D*: *Applied Physics* 2000; **33**:2268–2273.
17. Phelps AV. Excitation and ionization coefficients. In *Gaseous Di-electrics V*, Christophourou L, Bouldin DW (eds). Pergamon: New York, 1987.
18. Aleiferis PG, Taylor AMKP, Whitelaw JH, Ishii K, Urata Y. Cyclic variations of initial flame Kernel growth in a Honda Vtec-E lean-burn spark-ignition engine. *SAE Paper No. 2000-01-1207*, 2000.
19. Johansson B. Cycle to cycle variations in SI engines—the effects of fluid flow and gas composition in the vicinity of the spark plug on early combustion. *SAE Paper 962084*, 1996.
20. Kogoma M. Generation of atmospheric-pressure glow and its applications. *Journal of Plasma and Fusion Research* 2003; **79**(10):1000.
21. Phuoc T. Single-point versus multi-point laser ignition: experimental measurements of combustion times and pressures. *Combustion and Flame* 2000; **122**:508–510.

DOI: 10.1002/nme

22. Morsy MH, Ko YS, Chung SH, Cho P. Laser-induced two point ignition of premixture with a single-shot laser. *Combustion and Flame* 2001; **125**:724–727.
23. Morsy MH, Chung SH. Laser induced multi-point ignition with a single-shot laser using two conical cavities for hydrogen/air mixtures. *Experimental Thermal and Fluid Science* 2003; **27**:491–497.
24. Ma JX, Alexander DR, Poulain DE. Laser spark ignition and combustion characteristics of methane–air mixtures. *Combustion and Flame* 1998; **112**:492–506.
25. Ma JX, Ryan TW, Buckingham JP. Nd: YAG laser ignition of natural gas. *ASME*, *98-ICE-114*, 1998.
26. Mohamed AH, Block R, Schoenbach KH. Direct current discharges in atmospheric air. *IEEE Transactions on Plasma Science* 2002; **30**(1):182–183.
27. Weinberg FJ, Wilson JR. A preliminary investigation of the use of focused laser beams for minimum ignition energy studies. *Proceedings of the Royal Society of London* 1971; **A321**:41–52.
28. Dale JD, Smy PR, Clements RM. Laser ignited internal combustion engine—an experimental study. *SAE-780329*, Detroit, 1978.
29. Ronney PD. Laser versus conventional ignition of flames. *Optical Engineering* 1994; **33**(2):510.
30. Beduneau JL, Kim B, Zimmer L, Ikeda Y. Measurements of minimum ignition energy in premixed laminar methane/air flow by using laser induced spark. *Combustion and Flame* 2003; **132**:653–665.
31. Chen YL, Lewis JWL. Visualisation of laser-induced breakdown and ignition. *Optics Express* 2001; **9**(7):360–372.
32. Phuoc T. Laser spark ignition: experimental determination of laser-induced breakdown thresholds of combustion gases. *Optics Communication* 2000; **175**:419–423.
33. Kim Y, Ferreri VW, Rosocha LA, Anderson GK, Abbate S, Kim K-T. Effect of plasma chemistry on activated propane/air flames. *IEEE Transactions on Plasma Science* 2006; **34**(6):2532–2536.
34. Ombrello T, Ju Y. Ignition enhancement using magnetic gliding arc. *45th AIAA Aerospace Sciences Meeting and Exhibit*, Reno, NV, 8–11 January 2007 *AIAA Paper No. 2007-1025*.
35. Mintoussov E, Anokhin E, Starikovskii AY, Plasma-assisted combustion and fuel reforming. *45th AIAA Aerospace Sciences Meeting and Exhibit*, Reno, NV, 8–11 January 2007. *AIAA Paper No. 2007-1382*.
36. Korolev YD, Matveev IB. Nonsteady-state processes in a plasma pilot for ignition and flame control. *IEEE Transactions on Plasma Science* 2006; **34**(6):2507.
37. Esakov II, Grachev LP, Khodataev KV, Vinogradov VV, Van Wie DM. Propane–air mixture combustion assisted by MW discharge in a speedy airflow. *IEEE Transactions on Plasma Science* 2006; **34**(6):2497.
38. Linkenheil K, Ruoss RO, Heinrich W. Design and evaluation of a novel spark-plug based on a microwave coaxial resonator. *Microwave Conference 34th European*, *IEEE*, vol. 3(11–15), 2004; 1561–1564.
39. Linkenheil K, Ruoss HO, Grau T, Seidel J, Heinrich W. A novel spark-plug for improved ignition in engines with gasoline direct injection (GDI). *IEEE Transactions on Plasma Science* 2005; **33**(5):1696.
40. Ikeda Y, Nishiyama A, Kawahara N, Tomita E, Nakayama T. Local equivalence ratio measurement of CH_4/air and C_3H_8/air laminar flames by laser-induced breakdown spectroscopy. *44th AIAA Aerospace Sciences Meeting and Exhibit*, Reno, NV, 9–12 January 2006. *AIAA Paper No. 2006-965*.
41. Kawahara K, Ueda K, Ando H. Mixing control strategy for engine performance improvement in a gasoline direct-injection engine. *SAE Paper*, *No. 980158*, 1998.
42. Mehresh P, Souder J, Flowers D, Riedel U, Dibble RW. Combustion timing in HCCI engines determined by ion-sensor: experimental and kinetic modeling. *Proceedings of the Combustion Institute* 2005; **30**:2701–2709.
43. Bogin G, Chen JY, Dibble RW. The effects of intake pressure, fuel concentration, and bias voltage on the detection of ions in a homogeneous charge compression ignition (HCCI) engine. *Proceedings of the Combustion Institute* 2009; **32**(2):2877–2884.
44. Prager J, Riedel U, Warnatz J. Modeling ion chemsitry and charged species diffusion in lean methane–oxygen flames. *Proceedings of the Combustion Institute* 2007; **31**(1):1129–1137.
45. Zohdi TI. A computational framework for agglomeration in thermo-chemically reacting granular flows. *Proceedings of the Royal Society* 2004; **460**:3421–3445.
46. Zohdi TI. Modeling and direct simulation of near-field granular flows. *International Journal of Solids and Structures* 2004; **42/2**:539–564.
47. Zohdi TI. Charge-induced clustering in multifield particulate flow. *International Journal for Numerical Methods in Engineering* 2005; **62**(7):870–898.
48. Zohdi TI. *Introduction to the Modeling and Simulation of Particulate Flows*. SIAM: Philadelphia, PA, 2007.
49. Zohdi TI. Computation of strongly coupled multifield interaction in particle-fluid systems. *Computer Methods in Applied Mechanics and Engineering* 2007; **196**:3927–3950.

DOI: 10.1002/nme

50. Zohdi TI. On the computation of the coupled thermo-electromagnetic response of continua with particulate microstructure. *International Journal for Numerical Methods in Engineering* 2008; **76**:1250–1279.
51. Volland H. In *Atmospheric Electrodynamics in Physics in Chemistry and Space*, Lanzerotti LJ, Wasson JT (eds), vol. II. Springer: New York, 1984; 205.
52. Markson R. Ionospheric potential variations obtained from aircraft measurements of potential gradient. *Journal of Geophysical Research* 1976; **84**:161–200.
53. MacGorman DR, Rust WD. *The Electrical Nature of Thunderstorms*. Dover: New York, 1998.
54. Uman MA. The earth as a leakey spherical capacitor. *American Journal of Physics* 1974; **42**:1033–1035.
55. Zohdi TI. Genetic design of solids possessing a random-particulate microstructure. *Philosophical Transactions of the Royal Society*: *Mathematical*, *Physical and Engineering Sciences* 2003; **361**(1806):1021–1043.

DOI: 10.1002/nme